Collective behavior of biological aggregations in two dimensions: a nonlocal kinetic model

RAZVAN FETECAU*

August 16, 2010

Abstract

We construct and investigate a new nonlocal kinetic model for the formation and movement of animal groups in two dimensions. The model generalizes to two dimensions the one-dimensional hyperbolic model from [1]. The main modeling aspect in the present approach concerns the assumptions we make on the turning rates, to include, in a nonlocal fashion, the three types of social interactions that act among individuals of a group: attraction, repulsion and alignment. We show that solutions to the new mathematical model are bounded, along with their gradients. We also present numerical results to illustrate three types of group formations that we obtained with the new model, starting from random initial conditions : (i) swarms (aggregation into a group, with no preferred direction of motion), (ii) parallel/ translational motion (uniform spatial density, movement in a certain preferred direction) and (iii) parallel groups (aggregation into a group, with movement in a preferred direction).

Keywords: Two-dimensional swarms; non-local interactions; kinetic models.
AMS Subject Classification: 92D50, 35F20, 35Q92

1 Introduction

The mathematical modeling of collective behavior of biological aggregations (such as fish schools, ungulate herds, insect swarms, bird flocks) has received a great amount of interest in recent years. Nature offers spectacular formations of animal groups [2] (zigzagging flocks of birds [3] or milling schools of fish for instance [4, 5]) that have intrigued scientists, who tried to understand their formation and long-time behavior. On a practical level, understanding the collective behavior of animals could be useful in many instances, for example: provide fishing strategies [6, 7] or predict and control the devastating effects of desert locust outbreaks [8].

There are two main classes of mathematical models used for biological aggregations: 1) particle-based (Lagrangian) models, which track the movements of all individuals in the group, and 2) partial differential equations (PDE) models, formulated as evolution equations for the population density field. Some particle-based models are simply formulated in terms of decision rules that govern the evolution of each individual as it interacts with the other members of the group [9, 10]. Other models are given by a system of nonlinear ordinary differential equations for the positions and velocities of all individuals [11], typically expressing Newton's laws of motion [12, 13]. The size of the system is proportional to the number of individuals in the group, leading to limitations of

*Department of Mathematics, Simon Fraser University, 8888 University Dr., Burnaby, BC V5A 1S6, Canada

the Lagrangian approach in regards to solid analytical studies of the mathematical properties of the model. Nevertheless, computational studies of particle-based models revealed very interesting patterns and state transitions, that closely agree with various biological aggregations observed in nature [10, 12, 13].

The second approach casts the problem as a partial differential equation for the dynamics of the population density field. PDE models for aggregation can be classified into two categories: kinetic [14] and continuum (macroscopic). The latter category is better represented in the literature on biological aggregations, with a diverse range of parabolic [15, 16] and hyperbolic [1, 17, 18] models. Presently, there exits however a fast growing interest on kinetic models for aggregation and their corresponding hydrodynamic limits [19, 20, 21], along similar lines to the more established kinetic theory of gases [22]. Other recent works [23, 12] introduce macroscopic aggregation equations as continuum limits of individual based (microscopic) models and compare the results obtained with the two approaches. A very active line of research has focused recently on a high dimensional aggregation model described by the continuity equation for the population density field, where the velocity is assumed to have a prescribed functional dependence on the density [15, 16, 24, 25]. The functional dependence of the velocity on density typically incorporates nonlocal attraction and repulsion effects via convolution with a social interaction kernel. Our approach in this paper is different, as we include social interactions in turning rates.

The factors that can influence group formation can be external in nature, for example chemotactic, phototactic, thermotactic effects, or internal, such as the social interactions among individuals. The PDE aggregation models incorporate to various degrees such factors, that can be either local, where immediate neighbors or local environmental effects are important [26, 17], or nonlocal, where distant individuals and nonlocal factors play the dominant role [1, 15, 18, 16].

The present research deals with a two-dimensional, nonlocal kinetic model for animal aggregation that considers only internal interaction factors, such as attraction, repulsion and alignment. There are only a few works in the existing literature on PDE models for aggregation that deal with *both* the spatial and orientational aspects of interactions among individuals of a group. Alignment (angular orientation) interactions have been treated separately in various specific biological problems (e.g., self-organization of the actin cytoskeleton [27], fibroblast cultures [28], parallel alignment in myxobacteria swarms [29]) or in a more general framework in works such as [30, 31]. There are a few exceptions, when spatial dependence was considered, for example in the general study of the dynamic behavior of ensembles of "objects" [32] and in the one-dimensional aggregation model from [17].

This article introduces and investigates a two-dimensional extension of the nonlocal hyperbolic model for biological aggregations derived in [1] and further investigated in [33, 34]. The one-dimensional model from [1] consists in the following system of conservation laws for the right and left moving densities of individuals u^+ and u^-, respectively:

$$\partial_t u^+ + \partial_x(\gamma u^+) = -\lambda^+[u^+, u^-]u^+ + \lambda^-[u^+, u^-]u^-, \tag{1a}$$

$$\partial_t u^- - \partial_x(\gamma u^-) = \lambda^+[u^+, u^-]u^+ - \lambda^-[u^+, u^-]u^-. \tag{1b}$$

Here γ is a constant [1] speed, and λ^+ (λ^-) denote the turning rates of the individuals that were initially moving to the right (left) and then turn to change direction. The main merit of model (1) is that it takes into account *all* three social interactions (attraction, repulsion and alignment)

[1] A more recent work [35] considers nonlocal density-dependent speeds in (1).

that govern the response of an individual to signals perceived from its neighbors. The three social interactions are modeled by nonlocal terms that enter in the expressions of the turning rates $\lambda^{\pm}$. Model (1) was shown to capture a wide variety of spatial and spatiotemporal patterns [33]. Some of those patterns, such as traveling pulses or stationary pulses, are classical, and have been obtained with other models. Other patterns were new (ripples, zizgags, feathers and breathers [33]) and apparently emerged only as a result of interactions between all three social forces (attraction, repulsion and alignment).

The two-dimensional analogue of (1) introduced and studied in this article reads:

$$\partial_t u + \gamma \mathbf{e}_\phi \cdot \nabla_{\mathbf{x}} u = -\lambda(\mathbf{x}, \phi) u + \int_{-\pi}^{\pi} T(\mathbf{x}, \phi', \phi) u(\mathbf{x}, \phi', t) d\phi'. \tag{2}$$

Here $u(\mathbf{x}, \phi, t)$ is the total density of individuals at $\mathbf{x} = (x, y)$ moving in the direction $\phi \in (-\pi, \pi]$, measured from the positive axis x. Individuals move with constant speed γ in the direction $\mathbf{e}_\phi = (\cos\phi, \sin\phi)$. The function $\lambda(\mathbf{x}, \phi)$ describes the reorientation rate of individuals at $(\mathbf{x}, \phi)$ and the function $T(\mathbf{x}, \phi', \phi)$ describes the rate at which an individual located at $\mathbf{x}$ changes direction from ϕ' to ϕ after interaction with neighbors. The precise forms of λ and T are deferred to the next section[2]. Equation (4) expresses the fact that the change in the density of individuals at $(\mathbf{x}, \phi, t)$ is the result of two processes: (i) reorientation of individuals at $\mathbf{x}$ from ϕ to some other direction, encoded in the term $-\lambda u$ and (ii) orientation of individuals from directions ϕ' into ϕ, described by the integral term. Consistency between the definitions and interpretations of λ and T is contained in the following equation connecting them:

$$\lambda(\mathbf{x}, \phi) = \int_{-\pi}^{\pi} T(\mathbf{x}, \phi, \phi')\, d\phi'. \tag{3}$$

Indeed, $\lambda(\mathbf{x}, \phi)$, the turning rate from direction ϕ to *any* other direction should be obtained by integrating $T(\mathbf{x}, \phi, \phi')$, the turning rate from direction ϕ to ϕ', over all possible *new* directions ϕ'.

For constant turning rates λ, equation (2) can be reduced to a model of dispersal of organisms derived in [14] using a discrete stochastic approach called velocity jump process. In [14], the random velocity changes are the result of a Poisson process of intensity λ. Alternatively, λ^{-1} has the meaning of mean run length time between the random choices of direction. T has the interpretation of a turning kernel, providing the probability of a velocity jump from one velocity to another. The equation presented in [14] assumes a constant turning rate λ, but the authors mention that λ may depend on other variables as well. The model from [14] has attracted a fair amount of interest in the subsequent literature, but there have been no attempts to consider specific models for λ and T that incorporate social interactions and furthermore, no numerical experiments tested the capabilities of the model to capture biologically relevant features of animal aggregations. Some attempts to model two-dimensional group formations using density-dependent turning rates are presented very briefly in [29] and in the Appendix of [34]. We follow a different approach in the present article.

In our work we model the turning rate λ and the reorientation rate T to include *all* three social interactions (attraction, repulsion and alignment). We assume that λ depends non-locally on the density u via convolutions with interaction kernels. The three interactions are accounted for in an additive manner, each being represented by a distance and an orientation kernel acting at a

[2]Although not explicitly stated in the notation, the turning rates λ and T depend on the solution u itself, as their expressions involve integrals of the solution u, with weights given by the interaction kernels.

certain range (repulsion, alignment and attraction are assumed to act at short, intermediate and long distances, respectively). The reorientation rate T is modeled similarly, except that here we introduce turning probability functions to describe the likelihood of turning from one direction to another [27] as a result of interactions with neighbors. Section 2 contains the description of the mathematical model. Equation (2) has some readily available properties, such as conservation of mass (following from (3)) and boundedness of the solution and its gradients. We present these results in Section 3. Also in Section 3 we show how one can recover the one-dimensional model (1) from (2). Finally, in Section 4 we present numerical results that illustrate three types of group formations that we obtained with model (2), starting from random initial conditions : (i) swarms (aggregation into a group, with no preferred direction of motion), (ii) parallel/ translational motion (uniform spatial density, movement in a certain preferred direction) and (iii) parallel groups (aggregation into a group, with movement in a preferred direction).

2 Model Description

We restate the integro-differential equation

$$\partial_t u + \gamma \mathbf{e}_\phi \cdot \nabla_{\mathbf{x}} u = -\lambda(\mathbf{x}, \phi) u + \int_{-\pi}^{\pi} T(\mathbf{x}, \phi', \phi) u(\mathbf{x}, \phi', t) d\phi', \tag{4}$$

for the total density of individuals $u(\mathbf{x}, \phi, t)$, at space location $\mathbf{x} = (x, y)$ in the direction $\phi \in (-\pi, \pi]$, measured from the positive axis x. Individuals move with constant speed γ in the direction $\mathbf{e}_\phi = (\cos\phi, \sin\phi)$ and turn to approach, to avoid or to align with their neighbors. Turning is modeled by $\lambda(\mathbf{x}, \phi)$, which describes the reorientation rate of individuals at $(\mathbf{x}, \phi)$ and by $T(\mathbf{x}, \phi', \phi)$, which represents the rate at which an individual located at $\mathbf{x}$ changes direction from ϕ' to ϕ after interaction with neighbors [3].

The two terms, $\lambda(\mathbf{x}, \phi)$ and $T(\mathbf{x}, \phi', \phi)$, depend on the assumptions we make about how individuals interact with each other. Here, we will assume that these inter-individual interactions are influenced by two factors:

- *Distance from neighbors.* This results in three concentric, possibly overlapping, interaction zones for repulsion, alignment and attraction (see Figure 1)[4]. These zones can be modeled mathematically using distance kernels $K_j^d(\mathbf{x})$, $j = r, al, a$:

$$K_j^d(\mathbf{x}) = \frac{1}{A_j} e^{-(\sqrt{x^2+y^2} - d_j)^2/m_j^2}, \ j = r, al, a, \tag{5}$$

  where d_j describe the repulsion ($j = r$), alignment ($j = al$) and attraction ($j = a$) interaction ranges, and m_j gives the width of these ranges. The constant A_j ensures that each kernel integrates to 1:

$$A_j = \pi m_j \left(m_j e^{-d_j^2/m_j^2} + \sqrt{\pi} d_j + \sqrt{\pi} d_j \operatorname{erf}(d_j/m_j) \right).$$

[3] The right-hand-side of the model equation (4) is in the loss/ gain form reminiscent of the Bolzmann collision operator [22]. Bolzmann-type collisional mechanisms have been recently adapted to model velocity changes in bird flocking [36].

[4] Other works suggest alternative concepts of "distance". Recent studies [37, 38] on bird flocks propose as the relevant quantity the topological distance, defined as the number of individuals that separate two birds.

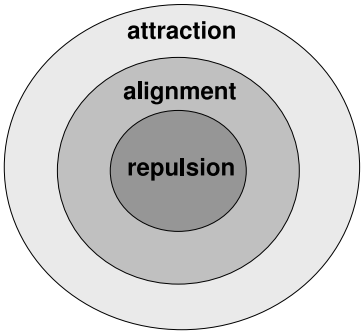

(a)

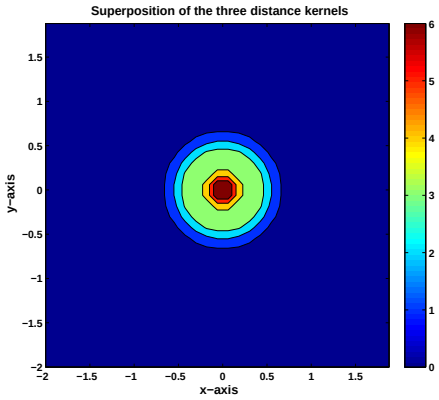

(b)

Figure 1: Interaction zones in 2D. (a) Generic interaction zones for an individual placed at the center of the three concentric circles that define its interaction ranges. (b) Contour plot of the superposition of the three ($j = r, al, a$) distance kernels given by (5). The values of the parameters correspond to Run 2 presented in the numerics section.

- *Neighbors' orientation.* The reference individual weighs the information it receives regarding the direction of movement of its neighbors, and then decides whether to change its direction (to avoid collision, to approach or to align with its neighbors). This behavior can be described mathematically using rotation kernels which depend on the movement direction ϕ and position $\mathbf{x}$ of the reference individual, as well as on the movement direction θ and position $\mathbf{s}$ of its neighbors.

Modeling the turning rate λ. We consider the social interactions between individuals (alignment, attraction, repulsion) to distinguish 3 mechanisms for turning:

(i) Turning to *align* with neighbors. An individual located at $\mathbf{x}$ moving in the direction ϕ changes its direction of motion due to interactions with individuals $\mathbf{s}$ in its alignment range. Suppose that the individual at $\mathbf{s}$ moves in the direction θ. We assume that individuals are less likely to turn if their neighbors are approximately moving in the same direction (i.e., $|\phi - \theta|$ small). In contrast, individuals are very likely to reorient themselves if their neighbors are moving in the opposite direction (i.e., $|\phi - \theta|$ large) — see Figure 2(a). Such a behavior can be described by the following function:

$$K^o_{al}(\theta;\phi) = \frac{1}{2\pi}\left(-\cos(\phi-\theta)+1\right). \tag{6}$$

Note that $K^o_{al}(\theta;\phi)$ is lowest ($=0$) if $\phi = \theta$, when the individuals are already aligned, and highest ($=1/\pi$) if $\phi = \theta \pm \pi$, when individuals move in opposite directions. We model the turning rate due to alignment only by the following nonlocal expression:

$$\lambda_{al}(\mathbf{x},\phi) = q_{al}\int_{\mathbb{R}^2}\int_{-\pi}^{\pi} K^d_{al}(\mathbf{x}-\mathbf{s})K^o_{al}(\theta;\phi)u(\mathbf{s},\theta,t)d\theta d\mathbf{s}, \tag{7}$$

where q_{al} is a constant that gives the strength of alignment. The alignment turning rate at $(\mathbf{x},\phi)$, as defined by (7), takes into account the densities $u(\mathbf{s},\theta)$ of its neighbors, with proper weights given by their distance from $\mathbf{x}$ (convolution with the distance alignment kernel K^d_{al}) and the likelihood of a turn, given by $K^o_{al}(\theta;\phi)$.

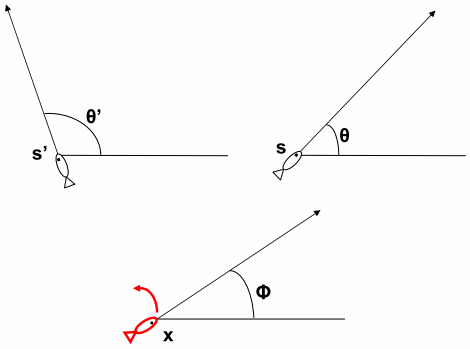

(a)

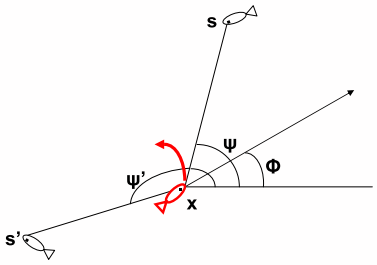

(b)

Figure 2: A generic individual located at $\mathbf{x}$ moving in the direction ϕ changes its direction of motion due to interactions with its neighbors. (a) Alignment interaction. The individuals at $\mathbf{s}$ and $\mathbf{s}'$ in the alignment range of $\mathbf{x}$ move in the directions θ and θ', respectively. The individual at $\mathbf{x}$ is more likely to turn due to its interaction with $\mathbf{s}'$ than with $\mathbf{s}$, as $|\phi - \theta'|$ is larger than $|\phi - \theta|$. (b) Attraction interaction. The individuals at $\mathbf{s}$ and $\mathbf{s}'$ are in the attraction range of $\mathbf{x}$. The individual at $\mathbf{x}$ is more likely to turn due to its interaction with $\mathbf{s}'$ than with $\mathbf{s}$, as $|\phi - \psi'|$ is larger than $|\phi - \psi|$.

(ii) Turning to approach individuals due to *attraction*. This turning mechanism depends on the movement direction ϕ of the reference individual located at $\mathbf{x}$ versus the position $\mathbf{s}$ of the neighbors inside the attraction range. We consider the relative location $\mathbf{s}-\mathbf{x}$ of the individual at $\mathbf{s}$ with respect to the reference individual and denote by ψ the angle that this vector makes with the positive x axis — see Figure 2(b). Provided $\mathbf{s}-\mathbf{x}=(s_x,s_y)$, the angle ψ is defined by

$$\cos\psi=\frac{s_x}{\sqrt{s_x^2+s_y^2}},\quad \sin\psi=\frac{s_y}{\sqrt{s_x^2+s_y^2}}. \tag{8}$$

The reference individual is more likely to turn to approach its neighbor at $\mathbf{s}$ provided $|\phi-\psi|$ is large ($\mathbf{s}$ is behind $\mathbf{x}$). On the other hand, the individual at $\mathbf{x}$ is less likely to turn provided $|\phi-\psi|$ is small ($\mathbf{s}$ is ahead of $\mathbf{x}$ and the reference individual maintains its direction of motion to meet $\mathbf{s}$) — see Figure 2(b). We use the following function to describe this behavior:

$$K_a^o(\mathbf{s};\mathbf{x},\phi)=\frac{1}{2\pi}\big(-\cos(\phi-\psi)+1\big). \tag{9}$$

Note that K_a^o does not depend on the direction of motion of the neighbor located at $\mathbf{s}$. If $\mathbf{s}$ is right ahead of $\mathbf{x}$ ($\psi=\phi$), $K_a^o(\mathbf{s};\mathbf{x},\phi)=0$, as there is no need to turn, as far as attraction is concerned. Moreover, $K_a^o(\mathbf{s};\mathbf{x},\phi)=1/\pi$, the highest possible value, provided $\mathbf{s}$ is right behind $\mathbf{x}$ ($|\psi-\phi|=\pi$). Introducing a constant q_a that describes the strength of attraction, the turning rate due to attraction only is modeled similarly to (7), by

$$\lambda_a(\mathbf{x},\phi)=q_a\int_{\mathbb{R}^2}\int_{-\pi}^{\pi}K_a^d(\mathbf{x}-\mathbf{s})K_a^o(\mathbf{s};\mathbf{x},\phi)u(\mathbf{s},\theta,t)d\theta d\mathbf{s}. \tag{10}$$

(iii) Turning to avoid individuals due to *repulsion*. This turning mechanism is the opposite of that for attraction. Using the same notations as above, a reference individual located at $\mathbf{x}$ that moves in the direction ϕ is very likely to turn to avoid encounters with neighbors $\mathbf{s}$ in its repulsion range, provided $|\phi-\psi|$ is small ($\mathbf{s}$ is ahead of $\mathbf{x}$) and less likely to turn provided $|\phi-\psi|$ is large ($\mathbf{s}$ is behind $\mathbf{x}$). Similarly, we introduce the function

$$K_r^o(\mathbf{s};\mathbf{x},\phi)=\frac{1}{2\pi}\big(\cos(\phi-\psi)+1\big), \tag{11}$$

and we model the turning rate due to repulsion by

$$\lambda_r(\mathbf{x},\phi)=q_r\int_{\mathbb{R}^2}\int_{-\pi}^{\pi}K_r^d(\mathbf{x}-\mathbf{s})K_r^o(\mathbf{s};\mathbf{x},\phi)u(\mathbf{s},\theta,t)d\theta d\mathbf{s}. \tag{12}$$

Here, the constant q_r gives the strength of repulsion.

Finally, by taking contributions from all three social interactions, the turning rate $\lambda(\mathbf{x},\phi)$ in (4) is defined as the sum:

$$\lambda(\mathbf{x},\phi)=\lambda_{al}(\mathbf{x},\phi)+\lambda_a(\mathbf{x},\phi)+\lambda_r(\mathbf{x},\phi). \tag{13}$$

Remark. Let us revisit (7), (10) and (12). Note that the kernels used in these definitions integrate to 1, that is,

$$\int_{\mathbb{R}^2}\int_{-\pi}^{\pi}K_{al}^d(\mathbf{x}-\mathbf{s})K_{al}^o(\theta;\phi)d\theta d\mathbf{s}=1, \tag{14}$$

$$\int_{\mathbb{R}^2}\int_{-\pi}^{\pi}K_j^d(\mathbf{x}-\mathbf{s})K_j^o(\mathbf{s};\mathbf{x},\phi)d\theta d\mathbf{s}=1,\qquad j=a,r \tag{15}$$

Equation (14) follows immediately from (5) and (6), as the space and angle integrals decouple, and both the distance and the orientation kernels integrate to 1. For the attraction kernel, use (8) and (9) to calculate, after expanding $\cos(\phi - \psi)$:

$$K_a^o(\mathbf{s}; \mathbf{x}, \phi) = \frac{1}{2\pi} \left(-\cos\phi \frac{s_x}{\sqrt{s_x^2 + s_y^2}} - \sin\phi \frac{s_y}{\sqrt{s_x^2 + s_y^2}} + 1 \right).$$

Hence, since $K_a^o(\mathbf{s}; \mathbf{x}, \phi)$ does not depend on θ and the distance kernel K_a^d integrates to 1, we have,

$$\int_{\mathbb{R}^2} \int_{-\pi}^{\pi} K_a^d(\mathbf{x} - \mathbf{s}) K_a^o(\mathbf{s}; \mathbf{x}, \phi) d\theta d\mathbf{s} =$$
$$-\cos\phi \underbrace{\int_{\mathbb{R}^2} K_a^d(\mathbf{x} - \mathbf{s}) \frac{s_x}{\sqrt{s_x^2 + s_y^2}} d\mathbf{s}}_{=0} + -\sin\phi \underbrace{\int_{\mathbb{R}^2} K_a^d(\mathbf{x} - \mathbf{s}) \frac{s_y}{\sqrt{s_x^2 + s_y^2}} d\mathbf{s}}_{=0} + 1.$$

Observe that the integrals multiplying $\cos\phi$ and $\sin\phi$ are zero, as the integrands are odd in the first and second coordinates, respectively. Equation (15) follows for $j = a$. Similarly for repusion.

Modeling the reorientation terms $T(\mathbf{x}, \phi', \phi)$. This term describes the rate at which an individual positioned at $\mathbf{x}$ changes its orientation from ϕ' to ϕ due to interaction with its neighbors — see Figure 3. We model the change in orientation using a turning probability function [27] $w(\phi' - \phi, \phi' - \theta)$ that gives the probability of turning from direction ϕ' to ϕ as a result of interactions with individuals located at/ moving at direction θ (the latter distinction will be made precise shortly).

Since w is a probability of reorientation, it yields 1 when integrated over all possible new directions ϕ:

$$\int_{-\pi}^{\pi} w(\phi' - \phi, \phi' - \theta)\, d\phi = 1. \tag{16}$$

As we account for the three types of social interactions, we have turning probability functions w_{al}, w_a and w_r corresponding to alignment, attraction and repulsion, respectively.

We consider the same turning mechanisms described in the previous paragraph and model the reorientation rates due to three types of interactions by

$$T_{al}(\mathbf{x}, \phi', \phi) = q_{al} \int_{\mathbb{R}^2} \int_{-\pi}^{\pi} K_{al}^d(\mathbf{x} - \mathbf{s}) K_{al}^o(\theta; \phi') w_{al}(\phi' - \phi, \phi' - \theta) u(\mathbf{s}, \theta, t) d\theta d\mathbf{s} \tag{17}$$

$$T_a(\mathbf{x}, \phi', \phi) = q_a \int_{\mathbb{R}^2} \int_{-\pi}^{\pi} K_a^d(\mathbf{x} - \mathbf{s}) K_a^o(\mathbf{s}; \mathbf{x}, \phi') w_a(\phi' - \phi, \phi' - \psi) u(\mathbf{s}, \theta, t) d\theta d\mathbf{s} \tag{18}$$

$$T_r(\mathbf{x}, \phi', \phi) = q_r \int_{\mathbb{R}^2} \int_{-\pi}^{\pi} K_r^d(\mathbf{x} - \mathbf{s}) K_r^o(\mathbf{s}; \mathbf{x}, \phi') w_r(\phi' - \phi, \phi' - \psi) u(\mathbf{s}, \theta, t) d\theta d\mathbf{s}. \tag{19}$$

Here, q_{al}, q_a and q_r are the constants introduced in (7), (10) and (12) to describe the strengths of alignment, attraction and repulsion, respectively.

The definitions (17)-(19) are in similar spirit to the modeling assumptions on λ's from (7), (10) and (12), except that the former set addresses specifically the turning probability functions. For

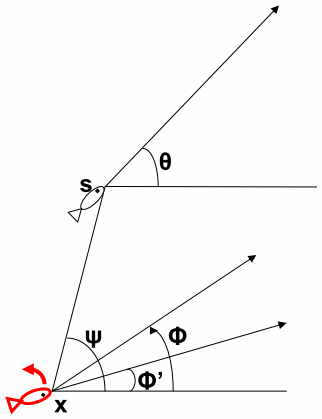

Figure 3: Reorientation mechanisms in 2D. An individual positioned at $\mathbf{x}$ changes its orientation from ϕ' to ϕ due to interaction with its neighbors. A generic neighbor is indicated by the individual located at $\mathbf{s}$ that moves in the direction θ. The reorientation mechanism in the figure may correspond to either alignment (the individual at $\mathbf{x}$ changes its direction to align with θ, the moving direction of $\mathbf{s}$) or attraction (the individual at $\mathbf{x}$ steers toward the location $\mathbf{s}$).

instance, the reorientation term $T_{al}(\mathbf{x}, \phi', \phi)$ defined by (17) considers the densities $u(\mathbf{s}, \theta)$ of its neighbors in the alignment range, with weights given by their distance from $\mathbf{x}$ (convolution with the distance alignment kernel K^d_{al}), the likelihood of a turn, given by $K^o_{al}(\theta; \phi)$, and the probability $w_{al}(\phi' - \phi, \phi' - \theta)$ that $(\mathbf{x}, \phi')$ changes direction to ϕ in order to align with θ, the moving direction of $\mathbf{s}$. For attraction and repulsion, the turning probabilities depend on the angle ψ that gives the relative location of $\mathbf{s}$ with respect to the reference individual located at $\mathbf{x}$.

Finally, $T(\mathbf{x}, \phi', \phi)$ includes the contributions from all social interactions:

$$T(\mathbf{x}, \phi', \phi) = T_{al}(\mathbf{x}, \phi', \phi) + T_a(\mathbf{x}, \phi', \phi) + T_r(\mathbf{x}, \phi', \phi). \tag{20}$$

Remark. The definitions and interpretations of the turning rates λ and T are consistent. Indeed, $\lambda(\mathbf{x}, \phi)$, the turning rate from direction ϕ to *any* other direction can be obtained by integrating $T(\mathbf{x}, \phi, \phi')$, the turning rate from direction ϕ to ϕ', over all possible *new* directions ϕ':

$$\lambda(\mathbf{x}, \phi) = \int_{-\pi}^{\pi} T(\mathbf{x}, \phi, \phi')\, d\phi'.$$

To obtain the equation above one has to use (16).

In fact, we could have used a more direct approach and introduce the turning rates T first (through formulas (17)-(19)), then simply define λ by the equation above. Hoping for a more transparent presentation, we preferred however a more gradual approach instead.

Modeling the probability functions w_{al}, w_a and w_r. We follow [27] and take the turning probability functions w_{al}, w_a and w_r in the form:

$$w(\phi' - \phi, \phi' - \theta) = g_\sigma(\phi' - \phi - v(\phi' - \theta)), \tag{21}$$

where g_σ is an approximation of the delta function with width σ and v is a *turning function*. With highest probability an individual moving in the direction ϕ' turns to direction

$$\phi = \phi' - v(\phi' - \theta),$$

due to its social interaction with another individual. Depending on the nature of interaction, θ can represent the direction of motion of the other individual (alignment) or the relative direction of the positions of the two individuals (attraction and repulsion).

The parameter $\sigma > 0$ measures the *uncertainty of turning* [27]. Larger σ means less exact turning, while σ very small indicates a very exact turning mechanism. Possible expressions for g_σ are: a periodic Gaussian or a normalized step function:

$$g_\sigma(\theta) = \frac{1}{\sqrt{\pi}\sigma} \sum_{z \in \mathbb{Z}} e^{-\left(\frac{\theta + 2\pi z}{\sigma}\right)^2}, \qquad \theta \in (-\pi, \pi), \tag{22}$$

$$g_\sigma(\theta) = \begin{cases} \frac{1}{2\sigma} & |\theta| < \sigma \\ 0 & \sigma < |\theta| \leq \pi. \end{cases} \tag{23}$$

Possible choices of the turning function v are discussed in [27] in the context of orientation of actin filaments. Among other choices we have

$$v(\theta) = \kappa \sin\theta, \tag{24}$$

$$v(\theta) = \kappa\theta, \tag{25}$$

where κ is a constant, $-1 \leq \kappa \leq 1$. Both cases give a certain rule for turning, either proportional to the sine of the relative angle or proportional to the relative angle itself. The sign of κ is very important, as it indicates if the orientation mechanism is attractive or repulsive, with $-1 \leq \kappa \leq 0$ for repulsive turning and $0 \leq \kappa \leq 1$ for attracting-like turning mechanisms (that includes attraction and alignment).

To conclude, the functions w_{al}, w_a and w_r have the form:

$$w_j(\phi' - \phi, \phi' - \theta) = g_{\sigma_j}(\phi' - \phi - v_j(\phi' - \theta)), \quad \text{with } j = al, a, r, \tag{26}$$

where the functions g_{σ_j} are approximations of the delta function with widths σ_j. The turning functions v_j (see (24) and (25)) involve a parameter κ_j, whose sign defines the type of interaction: non-negative for attraction-like interactions, i.e., $0 \leq \kappa_{al}, \kappa_a \leq 1$, and non-positive for repulsion-like ones, i.e., $-1 \leq \kappa_r \leq 0$. The magnitude of κ_j gives the extent to which an individual is attracted/ repelled by another individual's position or direction, while σ_j measures the uncertainty of turning due to the respective interaction.

3 Properties of the mathematical model

Conservation of mass. Integrate (4) over space $\mathbf{x} \in \mathbb{R}^2$ and angle $\phi \in (-\pi, \pi)$. The advection term in the left-hand-side renders 0 since u vanishes at infinity. Using (16) with the definitions of λ and T one concludes that the right-hand-side also renders 0, therefore yielding the conservation of the total mass:

$$\frac{d}{dt} \int_{\mathbb{R}^2} \int_{-\pi}^{\pi} u(\mathbf{x}, \phi, t) \; d\phi \, d\mathbf{x} = 0. \tag{27}$$

Denote by

$$M = \int_{\mathbb{R}^2} \int_{-\pi}^{\pi} u_0(\mathbf{x}, \phi) \; d\phi \, d\mathbf{x}, \tag{28}$$

the constant total mass.

Positivity of the solution. Note that, provided the initial data $u_0(\mathbf{x}, \phi)$ is non-negative, the solution to (4) remains non-negative for all times. Indeed, if u vanishes at $(\mathbf{x}, \phi, t)$, then its material derivative in the direction ϕ is non-negative

$$\begin{aligned} \frac{D}{Dt} u(\mathbf{x}, \phi, t) &= \int_{-\pi}^{\pi} T(\mathbf{x}, \phi', \phi) u(\mathbf{x}, \phi', t) d\phi' \\ &\geq 0, \end{aligned}$$

implying that u cannot drop below 0.

Boundedness of the solution. The left-hand-side of (4) is advection in the ϕ direction. We show below that the right-hand-side grows at most linearly in u and conclude from Gronwall's lemma that the solution remains bounded at all finite times. This rules out a finite-time density blow-up scenario driven for instance by a quadratic (of type u^2) right-hand-side. Indeed, from (17)-(20),

$$\begin{aligned} |T(\mathbf{x}, \phi', \phi)| &\leq C_1 \int_{\mathbb{R}^2} \int_{-\pi}^{\pi} u(\mathbf{x}, \phi, t) \; d\phi \, d\mathbf{x} \\ &= C_1 M, \end{aligned} \tag{29}$$

where

$$C_1 = 3 \max\{q_{al} \| K_{al}^d K_{al}^o w_{al} \|_{L^\infty}, q_a \| K_a^d K_a^o w_a \|_{L^\infty}, q_r \| K_r^d K_r^o w_r \|_{L^\infty}\}.$$

Hence,

$$\frac{D}{Dt} u(\mathbf{x}, \phi, t) \leq 2\pi C_1 M \| u(\cdot, \cdot, t) \|_{L^\infty(\mathbb{R}^2 \times (-\pi, \pi))}, \tag{30}$$

since the first term in the right-hand-side of (4) is non-positive. To simplify notations, let C denote the constant $2\pi M C_1$. We write (30) as

$$\frac{d}{dt} u(\mathbf{x} + t\gamma \mathbf{e}_\phi, \phi, t) \leq C \| u(\cdot, \cdot, t) \|_{L^\infty(\mathbb{R}^2 \times (-\pi, \pi))},$$

and after integration with respect to t we derive

$$u(\mathbf{x}+t\gamma\mathbf{e}_\phi,\phi,t) = u_0(\mathbf{x},\phi) + C\int_0^t \|u(\cdot,\cdot,t)\|_{L^\infty(\mathbb{R}^2\times(-\pi,\pi))}$$
$$\leq \|u_0\|_{L^\infty(\mathbb{R}^2\times(-\pi,\pi))} + C\int_0^t \|u(\cdot,\cdot,t)\|_{L^\infty(\mathbb{R}^2\times(-\pi,\pi))}.$$

The inequality holds for all $\mathbf{x}$, ϕ and t, therefore

$$\|u(\cdot,\cdot,t)\|_{L^\infty(\mathbb{R}^2\times(-\pi,\pi))} \leq \|u_0\|_{L^\infty(\mathbb{R}^2\times(-\pi,\pi))} + C\int_0^t \|u(\cdot,\cdot,t)\|_{L^\infty(\mathbb{R}^2\times(-\pi,\pi))},$$

for all t. Then, Gronwall's lemma gives finite time boundedess of the solution, provided the initial data is bounded:

$$\|u(\cdot,\cdot,t)\|_{L^\infty(\mathbb{R}^2\times(-\pi,\pi))} \leq \|u_0\|_{L^\infty(\mathbb{R}^2\times(-\pi,\pi))}\, e^{Ct}, \qquad \text{for all } t.$$

Boundedness of the gradients. A similar argument applies to the space-gradients of the solution, showing that shocks cannot occur in finite-time. Take a derivative with respect to x in (4) and denote $v = u_x$ to get

$$\partial_t v + \gamma\mathbf{e}_\phi\cdot\nabla_{\mathbf{x}} v = -\lambda_x u - \lambda v + \int_{-\pi}^{\pi} T_x(\mathbf{x},\phi',\phi)u(\mathbf{x},\phi',t)d\phi' + \int_{-\pi}^{\pi} T(\mathbf{x},\phi',\phi)v(\mathbf{x},\phi',t)d\phi'. \quad (31)$$

We show that the right-hand-side of (31) can grow at most linearly in v. Using conservation of the total mass (27) it follows easily that the turning rate λ from (13) is bounded by

$$|\lambda| \leq C_2 M,$$

with $C_2 = 3\max\{q_{al}\|K^d_{al}K^o_{al}\|_{L^\infty}, q_a\|K^d_a K^o_a\|_{L^\infty}, q_r\|K^d_r K^o_r\|_{L^\infty}\}$. Hence,

$$|\lambda v| \leq C_2 M\|v(\cdot,\cdot,t)\|_{L^\infty(\mathbb{R}^2\times(-\pi,\pi))}.$$

Also, using (29) we derive

$$\left|\int_{-\pi}^{\pi} T(\mathbf{x},\phi',\phi)v(\mathbf{x},\phi',t)d\phi'\right| \leq 2\pi C_1 M\|v(\cdot,\cdot,t)\|_{L^\infty(\mathbb{R}^2\times(-\pi,\pi))}.$$

Regarding the first term in the right-hand-side of (31), we calculate

$$\lambda_x = \lambda_{al,x} + \lambda_{a,x} + \lambda_{r,x}.$$

From (7),

$$|\lambda_{al,x}| \leq q_{al}\|K^d_{al,x}\|_{L^\infty}\|K^o_{al}\|_{L^\infty}M.$$

Also, from (10),

$$\lambda_{a,x} = q_a\int_{\mathbb{R}^2}\int_{-\pi}^{\pi}\left(K^d_{a,x}(\mathbf{x}-\mathbf{s})K^o_a(\mathbf{s};\mathbf{x},\phi) + K^d_a(\mathbf{x}-\mathbf{s})K^o_{a,x}(\mathbf{s};\mathbf{x},\phi)\right)u(\mathbf{s},\theta,t)d\theta d\mathbf{s}. \quad (32)$$

The distance kernels (5) are exponentially decreasing functions, therefore their derivatives are bounded and the first term in the right-hand-side of (32) can be bounded by

$$q_a \|K_{a,x}^d\|_{L^\infty} \|K_a^o\|_{L^\infty} M.$$

Regarding the second term, differentiate (9) with respect to x and use (8) to get,

$$\begin{aligned} K_{a,x}^o(\mathbf{s};\mathbf{x},\phi) &= -\frac{1}{2\pi}\sin(\phi-\psi)\frac{s_y}{s_x^2+s_y^2} \\ &= -\frac{1}{2\pi}\sin(\phi-\psi)\sin\psi\,\frac{1}{|\mathbf{s}-\mathbf{x}|}, \end{aligned}$$

where we remind the reader that $\mathbf{s}-\mathbf{x} = (s_x, s_y)$. Note that $K_{a,x}^o$ is a singular, but integrable kernel. By passing to polar coordinates with origin at $\mathbf{x}$, the singular component $1/|\mathbf{s}-\mathbf{x}|$ goes away, leaving a bounded term. Finally, using the finite-time boundedness of u derived in the previous paragraph, the second term in (32) can be bounded by

$$C\|u\|_{L^\infty} \|K_a^d(|\mathbf{x}|)\|_{L^1(\mathbb{R})},$$

and combined with the previous result, we conclude that $|\lambda_{a,x}|$ is bounded. Boundedness of $\lambda_{r,x}$ follows similarly. Therefore, λ_x stays bounded at finite times.

Now return to the first term in the right-hand-side of (31) and use the boundedness of u to conclude that $|\lambda_x u|$ remains bounded at finite times. We omit to show the boundedness of the third-term in the right-hand-side of (31), as the derivation involves similar arguments.

Collecting the results, we get

$$\frac{D}{Dt} v(\mathbf{x},\phi,t) \le C(T)\|v(\cdot,\cdot,t)\|_{L^\infty(\mathbb{R}^2\times(-\pi,\pi))},$$

for all $t \in [0,T]$, with T arbitrary. Gronwall's lemma provides the boundedness at finite times of $v = u_x$. As a similar estimate can be derived for u_y, we conclude that $\|\nabla_{\mathbf{x}} u(\cdot,\cdot,t)\|_{L^\infty(\mathbb{R}^2\times(-\pi,\pi))}$ remains bounded for finite times, provided the initial data has a bounded gradient.

Finally, similar Growall-type arguments can be used to argue that $\|u_\phi(\cdot,\cdot,t)\|_{L^\infty(\mathbb{R}^2\times(-\pi,\pi))}$ remains bounded for finite times, provided u_ϕ is bounded initially.

Global existence of solutions. Local existence and uniqueness of solutions to equation (4) can be shown using standard fixed point arguments or the vanishing viscosity method. The a priori $W^{1,\infty}$ estimates derived in the previous paragraphs can then be used with a standard continuation principle to extend the local solutions globally in time. More precisely, one can conclude that given an initial datum $u_0 \in C^1 \cap W^{1,\infty}(\mathbb{R}^2 \times (-\pi,\pi))$ for equation (4), then for every $T > 0$, there exists a unique classical solution $u \in C^1 \cap W^{1,\infty}(\mathbb{R}^2 \times (-\pi,\pi) \times [0,T))$ to the aggregation model (4).

Reduction to other models. Denote by $\rho(\mathbf{x},t)$ the spatial density of individuals at location $\mathbf{x}$ and time t, that is

$$\rho(\mathbf{x},t) = \int_{-\pi}^{\pi} u(\mathbf{x},\phi,t)\, d\phi. \tag{33}$$

The velocity in the direction ϕ is $\gamma \mathbf{e}_\phi$, where γ is the constant speed and $\mathbf{e}_\phi = (\cos\phi, \sin\phi)$ is the unit vector in the direction ϕ. Define the average velocity $\mathbf{v}(\mathbf{x}, t)$ at $(\mathbf{x}, t)$ by

$$\rho(\mathbf{x}, t)\mathbf{v}(\mathbf{x}, t) = \int_{-\pi}^{\pi} \gamma \mathbf{e}_\phi u(\mathbf{x}, \phi, t)\, d\phi. \tag{34}$$

Integrating the equation of motion (4) with respect to ϕ one gets

$$\rho_t + \nabla_{\mathbf{x}} \cdot (\rho \mathbf{v}) = 0, \tag{35}$$

as the right-hand-side of (4) yields 0 after integration.

Similarly, multiply (4) by $\gamma \mathbf{e}_\phi$, integrate with respect to ϕ and derive an evolution equation for $\rho\mathbf{v}$:

$$\begin{aligned}(\rho\mathbf{v})_t + \gamma^2 \nabla_{\mathbf{x}} \cdot \int_{-\pi}^{\pi} u\, \mathbf{e}_\phi \otimes \mathbf{e}_\phi\, d\phi = \\ - \gamma \int_{-\pi}^{\pi} \lambda(\mathbf{x}, \phi) u(\mathbf{x}, \phi, t)\, \mathbf{e}_\phi d\phi + \gamma \int_{-\pi}^{\pi} \int_{-\pi}^{\pi} T(\mathbf{x}, \phi', \phi) u(\mathbf{x}, \phi', t)\, \mathbf{e}_\phi d\phi' d\phi,\end{aligned} \tag{36}$$

where $\otimes$ denotes tensor product.

Reduction to $1D$. Consider the one-dimensional problem, where individuals move along the x-axis in the only two admissible directions, that is $\phi = 0$ and $\phi = \pi$. The solution $u(x, \phi, t)$ is then in the form:

$$u(x, \phi, t) = u^+(x, t)\delta(\phi) + u^-(x, t)\delta(\phi - \pi), \tag{37}$$

where u^+ and u^- denote the densities of individuals that move right and left, respectively.

Plug (37) into (33) to get the total density in both directions:

$$\rho(x, t) = u^+(x, t) + u^-(x, t).$$

Similarly, from (37) and (34), the (horizontal) average momentum is

$$\rho(x, t)v(x, t) = \gamma u^+(x, t) - \gamma u^-(x, t). \tag{38}$$

Here we used that in 1D, for the two directions of motions (right-moving with $\phi = 0$ and left-moving with $\phi = \pi$), we have, respectively

$$\mathbf{e}_0 = 1 \qquad \text{and} \qquad \mathbf{e}_\pi = -1. \tag{39}$$

The continuity equation (35) then becomes

$$(u^+ + u^-)_t + \gamma(u^+ - u^-)_x = 0. \tag{40}$$

We now turn to the one-dimensional version of (36). We plug the one-dimensional solution (37) into (36) and use (39). The second term in the left-hand-side simply becomes

$$\gamma^2 \left(u^+(x, t) + u^-(x, t)\right)_x. \tag{41}$$

The first and second integrals in the right-hand-side of (36) yield, respectively,

$$- \gamma\lambda(x, 0)u^+(x, t) + \gamma\lambda(x, \pi)u^-(x, t), \tag{42}$$

and

$$\gamma \int_{-\pi}^{\pi} \left(T(x,0,\phi) u^+(x,t) + T(x,\pi,\phi) u^-(x,t) \right) \mathbf{e}_\phi d\phi. \tag{43}$$

We first look at the alignment components in (42) and (43). Before starting the calculation, let us inspect the alignment components of the first terms in (42) and (43). In $1D$ the set of directions $\mathbf{e}_\phi$ is discrete (see (39)). We expect $T_{al}(x,0,0) = 0$, as the right-moving individuals do not turn to remain aligned with the other right-movers. Therefore, the only non-trivial contribution from the first term in (43) comes from $\phi = \pi$. From (39), $\mathbf{e}_\pi = -1$. Also, $T_{al}(x,0,\pi)$ represents the turning rate due to alignment of the right-moving individuals, so it equals $\lambda_{al}(x,0)$. Based on these considerations we conclude that, upon summation, the alignment components of the first terms in (42) and (43) combine. Similar arguments hold for the second terms and also, for repulsion and attraction components, leading to the final outcome (46). Below we present the calculations that validate these intuitive considerations.

From (7) and (37) we calculate the alignment component of the turning rate λ,

$$\lambda_{al}(x,\phi) = q_{al} \left(K^0_{al}(0;\phi) \int K^d_{al}(x-s) u^+(s,t)\, ds + K^0_{al}(\pi;\phi) \int K^d_{al}(x-s) u^-(s,t)\, ds \right).$$

Using (6) we compute

$$\lambda_{al}(x,0) = q_{al} \frac{1}{\pi} \int K^d_{al}(x-s) u^-(s,t)\, ds, \tag{44}$$

as $K^o_{al}(0;0) = 0$ and $K^o_{al}(\pi;0) = 1/\pi$. Similarly,

$$\lambda_{al}(x,\pi) = q_{al} \frac{1}{\pi} \int K^d_{al}(x-s) u^+(s,t)\, ds. \tag{45}$$

The alignment components of $T(x,0,\phi)$ and $T(x,\pi,\phi)$ can be computed from (17), using (37):

$$T_{al}(x,0,\phi) = q_{al} \frac{1}{\pi} \int K^d_{al}(x-s) w_{al}(0-\phi, 0-\pi) u^-(s,t)\, ds,$$

and

$$T_{al}(x,\pi,\phi) = q_{al} \frac{1}{\pi} \int K^d_{al}(x-s) w_{al}(\pi-\phi, \pi-0) u^+(s,t)\, ds,$$

where we used $K^o_{al}(0;0) = K^o_{al}(\pi;\pi) = 0$ and $K^o_{al}(\pi;0) = K^o_{al}(0;\pi) = 1/\pi$.

Assume that an individual changes direction whenever it interacts with an individual moving in the opposite direction. This implies that the turning probability function w_{al} has the form:

$$w_{al}(\phi' - \phi, \phi' - \theta) = \delta(\phi - \phi' - \pi), \qquad \text{when } \phi' \neq \theta.$$

The equation expresses the fact that an individual that moves in the direction ϕ' interacts with an individual that moves in the opposite direction θ and as a result it turns and changes its direction to $\phi = \phi' + \pi$. As we work in the one-dimensional setting, ϕ', ϕ and θ take values only in the set $\{0, \pi\}$. As a result,

$$T_{al}(x,0,\phi) = \delta(\phi - \pi) q_{al} \frac{1}{\pi} \int K^d_{al}(x-s) u^-(s,t)\, ds,$$

$$T_{al}(x,\pi,\phi) = \delta(\phi) q_{al} \frac{1}{\pi} \int K^d_{al}(x-s) u^+(s,t)\, ds.$$

From (44) and (45) we further infer that

$$T_{al}(x,0,\phi) = \delta(\phi-\pi)\lambda_{al}(x,0)$$
$$T_{al}(x,\pi,\phi) = \delta(\phi)\lambda_{al}(x,\pi),$$

and upon substitution in (43) with use of (39) we conclude that the alignment component of the expression given by (43) equals that of (42).

Hence the alignment components of (42) and (43) combine and contribute to the right-hand-side of (36) the expression:

$$-2\gamma\lambda_{al}(x,0)u^+(x,t) + 2\gamma\lambda_{al}(x,\pi)u^-(x,t).$$

As a similar result holds for the attraction and repulsion components (we included these calculations in the Appendix), we conclude that the right-hand-side of (36) is given by

$$-2\gamma\lambda(x,0)u^+(x,t) + 2\gamma\lambda(x,\pi)u^-(x,t). \tag{46}$$

Make the notations

$$\lambda^+ = \lambda(x,0) \qquad \text{and} \qquad \lambda^- = \lambda(x,\pi),$$

for the turning rates of the individuals that move right and left, respectively.

Collecting (38), (41) and (46), we finally derive the one-dimensional version of (36) to be

$$\left(u^+ - u^-\right)_t + \gamma\left(u^+ + u^-\right)_x = -2\lambda^+u^+ + 2\lambda^-u^-. \tag{47}$$

By adding and subtracting the continuity equation (40) and the momentum equation (47) one recovers the one-dimensional model (1), introduced and studied in [1, 33].

Special $1D$ solutions.

1. *Alignment only.* Suppose alignment is the only social interaction between individuals ($q_a = q_r = 0$) and consider a two-dimensional motion along two opposite directions only, say the horizontal directions $\phi = 0$ and $\phi = \pi$. Assume the solution u does not depend on the y variable, that is

$$u(\mathbf{x},\phi,t) = u^+(x,t)\delta(\phi) + u^-(x,t)\delta(\phi-\pi). \tag{48}$$

The average momentum, as computed from (34), is horizontal:

$$\rho(\mathbf{x},t)\mathbf{v}(\mathbf{x},t) = (\gamma u^+(x,t) - \gamma u^-(x,t), 0)^T, \tag{49}$$

where we used

$$\mathbf{e}_0 = (1,0)^T \qquad \text{and} \qquad \mathbf{e}_\pi = (-1,0)^T.$$

Then follow a similar procedure as above and plug (48), (49) into (35) and (36). The key observation is that the space and angle variables decouple in the calculations. The turning rates continue do depend on the locations of individuals in the alignment range, but the turning is essentially a one-dimensional process (from right to left or viceversa). Hence one can derive two-dimensional versions of the density equation (40) and of the momentum equation (47), where the momentum equation is a trivial identity in the vertical direction and the divergence $\nabla_{\mathbf{x}}\cdot$ is simply the derivative with respect to the horizontal space variable x.

Therefore, we can simply add a vertical dimension to the the one-dimensional solutions of (1) and recover solutions of the system (4), the latter being considered in the particular case when alignment is the only interaction force between individuals.

If attraction and repulsion are considered as social interactions, this observation no longer holds. In this case turning is genuinely two-dimensional, as individuals turn to meet or avoid individuals in their range of attraction/ repulsion.

2. *Translational solution.* Provided alignment is the only social interaction ($q_a = q_r = 0$), system (4) admits a purely translational solution. Indeed, consider the initial data

$$u(\mathbf{x}, \phi, 0) = u_0(\mathbf{x})\delta(\phi),$$

where $u_0(\mathbf{x})$ has compact support $\Omega \subset \mathbb{R}^2$. We show that its translation with speed γ in the direction $\mathbf{e}_0$,

$$u(\mathbf{x}, \phi, t) = u_0(\mathbf{x} - \gamma \mathbf{e}_0 t)\delta(\phi), \tag{50}$$

is a solution of (4). Inspecting (4), we infer that it is sufficient to show that its right-hand-side vanishes at all ϕ. The first term in the right-hand-side is 0, as

$$\lambda_{al}(\mathbf{x}, \phi) = q_{al} K^o_{al}(0; \phi) \int_{\mathbb{R}^2} K^d_{al}(\mathbf{x} - \mathbf{s}) u_0(\mathbf{x} - \gamma \mathbf{e}_0 t)\, d\mathbf{s},$$

and taking its product with $u(\mathbf{x}, \phi, t)$ from (50) it yields the factor

$$K^o_{al}(0; \phi)\delta(\phi) = 0.$$

Here, we used $K^o_{al}(0; 0) = 0$. The second term in the right-hand-side of (4) is 0 as well. Indeed, calculate

$$\int_{-\pi}^{\pi} T_{al}(\mathbf{x}, \phi', \phi) u(\mathbf{x}, \phi', t) d\phi' = T_{al}(\mathbf{x}, 0, \phi) u_0(\mathbf{x} - \gamma \mathbf{e}_0 t).$$

Using (17) and (50), we further infer that

$$T_{al}(\mathbf{x}, 0, \phi) = 0,$$

as its expression includes the factor $K^o_{al}(0; 0) = 0$.

Case $\lambda = const$. For constant turning rates, $\lambda(\mathbf{x}, \phi) = \lambda$, and $T(\mathbf{x}, \phi', \phi) = \lambda \tilde{T}(\mathbf{x}, \phi', \phi)$, our model (4) reduces to

$$\partial_t u + \gamma \mathbf{e}_\phi \cdot \nabla_{\mathbf{x}} u = -\lambda u + \lambda \int_{-\pi}^{\pi} \tilde{T}(\mathbf{x}, \phi', \phi) u(\mathbf{x}, \phi', t) d\phi'. \tag{51}$$

This model was derived in [14] using a discrete stochastic approach called velocity-jump process. In [14], the random velocity changes are the result of a Poisson process of intensity λ (alternatively, λ^{-1} has the meaning of the mean run time between the random choices of direction). The function $\tilde{T}(\mathbf{x}, \phi', \phi)$ in [14] represents the probability of a change in direction from ϕ' to ϕ, similar to our turning probability functions w_j, $j = al, a, r$ from (26). There has been a fairly extensive amount of literature [1, 27, 34] dedicated to the dispersal model from [14], but no research except the present work attempted to include nonlocal social interactions in the turning rates and also, present numerical results to test the model in higher dimensions.

4 Numerical results

Numerical method. The definitions of λ and T involve space and angle convolutions of the distance and orientation kernels with the solution. For numerical purposes, Fourier methods provide an excellent means for calculating convolution integrals, rendering significant computational advantages over quadrature methods for instance. To calculate a convolution numerically, one simply performs a multiplication in the discrete Fourier space:

$$\widehat{K * u}\,(l) = \hat{K}(l)\hat{u}(l).$$

In addition, Fourier methods conveniently handle linear terms. Upon applying the $2D$ Fourier transform to the linear convective term in the left-hand-side of (4), we obtain

$$\gamma(\cos\phi\, l_1 + \sin\phi\, l_2)\hat{u},$$

where l_1 and l_2 are the horizontal and vertical components of the wavenumber, respectively. The resulting expression above is now algebraic and is being dealt with using the integrating factor method.

To advance the solution in time we use the 4th order Runge-Kutta method. For space discretization we use a rectangular grid on $[-L/2, L/2)\times[-L/2, L/2)$ with N^2 points, $\Delta x = \Delta y = L/N$. For angle discretization we use an equidistant grid on $[-\pi, \pi)$ with M points, $\Delta\phi = 2\pi/M$. To avoid aliasing, all multiplications of Fourier modes are done on an extended spatial grid of size $\left(\frac{3}{2}N\right)^2$ and an angular grid of size $\frac{3}{2}M$. The procedure is standard [39]: the extension is done by padding the spectrum matrix with zeros, calculations are performed in the extended space and then the spectrum is restricted back to the original size.

We give some brief details regarding the implementation of discrete convolutions used to compute the turning rates. The integral defining λ_{al} in (7) (see also (6)) represents a convolution in space and angle and it is trivial to compute its discrete Fourier spectrum. The integrals that define λ_a and λ_r in (10) and (12) (see also (9), (11) and (8)) however represent a convolution in space only. To see this, expand K_a^o from (9), using (8):

$$\begin{aligned} K_a^o(\mathbf{s};\mathbf{x},\phi) &= \frac{1}{2\pi}(-\cos\phi\cos\psi - \sin\phi\sin\psi + 1) \\ &= \frac{1}{2\pi}\left(-\cos\phi\frac{s_x}{s_x^2+s_y^2} - \sin\phi\frac{s_y}{s_x^2+s_y^2} + 1\right), \end{aligned}$$

where s_x and s_y are the x and y components of the relative position $\mathbf{s}-\mathbf{x}$. Therefore, the product $K_a^d K_a^o$ that enters in the integrand of (10) is only a function of $\mathbf{x}-\mathbf{s}$ and we can write

$$\lambda_a(\mathbf{x},\phi) = q_a \int_{\mathbb{R}^2} K_a^d(\mathbf{x}-\mathbf{s}) K_a^o(\mathbf{s};\mathbf{x},\phi) \int_{-\pi}^{\pi} u(\mathbf{s},\theta,t)\, d\theta\, d\mathbf{s}.$$

The θ-integral is the zero-mode (with respect to angle) of u, and the remaining space integral is a convolution. Similarly for λ_r.

We explain now briefly the calculation of the reorientation terms included in T. The integral defining $T_{al}(\mathbf{x},\phi',\phi)$ in (17) is clearly a convolution in space and angle. The integrals in (18)

and (19) that define $T_a(\mathbf{x}, \phi', \phi)$ and $T_r(\mathbf{x}, \phi', \phi)$ also represent convolutions (but in space only!), provided we use the turning functions v_a and v_r in the form (24). Indeed, for every ϕ' and ϕ fixed,

$$\begin{aligned} w_a(\phi' - \phi, \phi' - \psi) &= g_{\sigma_a}(\phi' - \phi - \kappa_a \sin(\phi' - \psi)) \\ &= g_{\sigma_a}\left(\phi' - \phi - \kappa_a(\sin\phi' \cos\psi - \cos\phi' \sin\psi)\right) \\ &= g_{\sigma_a}\left(\phi' - \phi - \kappa_a\left(\sin\phi' \frac{s_x}{s_x^2 + s_y^2} - \cos\phi' \frac{s_y}{s_x^2 + s_y^2}\right)\right), \end{aligned}$$

is a function of $\mathbf{x} - \mathbf{s}$. Hence, using the observation above regarding K_a^o we conclude that the integral in (18) is a convolution in the space variable. Similarly for $T_r(\mathbf{x}, \phi', \phi)$.

Numerical experiments. In all numerical simulations we take $L = 4$ and speed $\gamma = 1$. We take g_{σ_j}, $j = al, a, r$ from (26) in the form of a periodic Gaussian (22) with widths $\sigma_j = 0.2$, $j = al, a, r$, and the turning functions v_j, $j = al, a, r$, in the form (24). We fix the parameters that define the distance kernels (5): the interaction ranges $d_r = 0$, $d_{al} = 0.4$, $d_a = 0.8$ and the widths of the interaction ranges $m_r = 0.2$, $m_{al} = 0.2$, $m_a = 0.2$ — see also Figure 1. The numerical experiments presented below use $N = 65$, $K = 64$ and $\Delta t = 0.05$.

Run 1 (aggregation): Random in space and direction initial data (at every space location and angle direction the initial data is produced by a uniform random number generator). The parameters that give the strength of interactions are: $q_r = 1$, $q_{al} = 1$, $q_a = 5$. The proportionality constants that describe the amount or turning are: $k_r = -0.1$, $k_{al} = 0.1$, $k_a = 0.9$. Attraction is the dominant social interaction between individuals. After a certain time, the individuals aggregate in a group with well defined boundaries.

The contour plot of the spatial density $\rho(\mathbf{x}, t)$ (see (33)) at $t = 35$ is shown in Figure 4(a). As alignment is relatively weak, all directions are almost equally preferred, corresponding to a state of swarming. This can be observed in Figure 4(b) where we plot the density $u(\mathbf{x}, \phi, t)$ as a function of the orientation angle ϕ at $t = 35$ and $\mathbf{x}$ fixed at four space locations. The first space location is the center of the swarm, where the density is highest (solid line). The other three space locations are horizontal translations of the center of the swarm, to the right, by $3\Delta x$, $6\Delta x$ and $9\Delta x$, corresponding to the dashed, dotted and dash-dotted lines, respectively. The density decreases as the points approach the edge of the swarm, as reflected by the amplitudes of the four curves in the figure. Note that there is no preferred direction of motion at the center of the swarm. Toward the right edge of the swarm (dotted and dash-dotted lines) preference is given to motion in the negative horizontal direction $\phi = \pi$, as individuals move to preserve the aggregate. The solution settles into a steady state corresponding to a motionless swarm where individuals move in all directions.

A very interesting account on the various insect swarms observed in nature is given in [40] (see also references therein). Special techniques designed to track individual trajectories of mosquitos in a swarm showed that individuals do not seem to have preferred positions within a swarms, but appear to drift at random. The concentration distribution of the swarming insects (Figure 7.6 in [40]) has a bell-like shape, i.e., it is symmetric with respect to the swarm center, with high concentration in the center that decays to zero toward the edges. More specifically, [41] reports studies on the male swarms of *Anopheles gambiae*, a mosquito species that includes the most important vectors of malaria. Male mosquitos form swarms for mating purposes: the swarms attracts inseminated females, increasing the probability of efficient sexual encounters. It has been observed that swarms in this species are approximately spherical, "with an unexpectedly high

density of individuals close to the swarm centroid". Figure 4 captures all the features mentioned above: random drift, symmetrical shape and high density at the center.

Figure 4 may also correspond to the formation of a "bait ball", a tightly packed school of small fish (such as sardines) that forms under the threat of predation. An example of such pattern is offered by [42], which reported how under the threat of predation, a school of fish collapsed into a tight ball which became almost motionless. Note in Figure 4 that, despite the fact that the individuals in the swarm keep moving in all directions, the (macroscopic) swarm reaches a steady state, with a fixed center and shape.

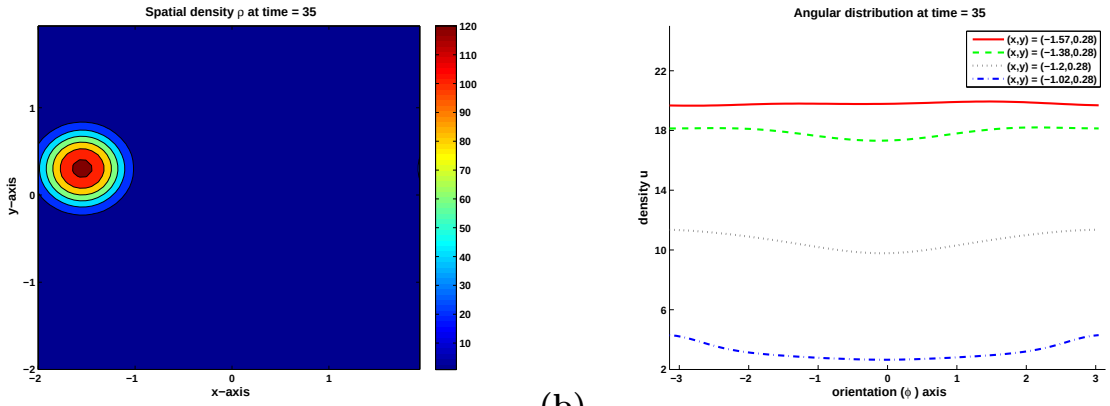

(a) (b)

Figure 4: Run 1(attraction dominated): $q_r = 1$, $q_{al} = 1$, $q_a = 5$, $k_r = -0.1$, $k_{al} = 0.1$, $k_a = 0.9$. The initial data is randomly generated in space and direction. (a) Contour plot of the spatial density ρ at $t = 35$. Note the formation of a group at $t = 35$. (b) Plot of the density u as a function of angle ϕ at $t = 35$ at four space locations. The first space location is the center of the swarm (solid line). The other three space locations are horizontal translations of the center of the swarm, to the right, by $3\Delta x$, $6\Delta x$ and $9\Delta x$, corresponding to the dashed, dotted and dash-dotted lines, respectively. There is no preferred direction at motion at the center of the swarm. Towards the right edge of the swarm (dotted and dash-dotted lines), preference is given to the negative horizontal direction $\phi = \pi$, in order to maintain the aggregate.

Run 2 (translation): The initial density is the constant 1 plus a uniform number generator in space and angle. The parameters are $q_r = 1$, $q_{al} = 3$, $q_a = 1$ and $k_r = -0.25$, $k_{al} = 0.75$, $k_a = 0.25$. Note that attraction and repulsion have equal strength that is smaller than the strength of alignment. This is an alignment dominated interaction, where individuals eventually align their motion along a preferred direction (translational solution). As attraction and repulsion balance each other, the individuals spread uniformly in the computational domain.

In Figure 5(a) we show the contour plot of $\rho(\mathbf{x}, t)$ at time $t = 48$. The distribution of the individuals is almost uniform in the domain. In Figure 5(b) we plot the angular distribution of the solution u at a fixed space location at times $t = 0$, 6, 14 and 48. Note the peak around $\phi = 1.37$ radians (about 78.75 degrees) and the drop to 0 in the other directions, indicating an almost [5] translational solution. We plot the solution at $t = 48$, but in fact there is no noticeable change

[5] We also captured numerically genuine translational solutions of (4) when alignment is the only social interaction between individuals ($q_a = q_r = 0$). This solutions were discussed in Section 3, see equation (50). Since this is virtually a one-dimensional motion, we did not include these numerical results.

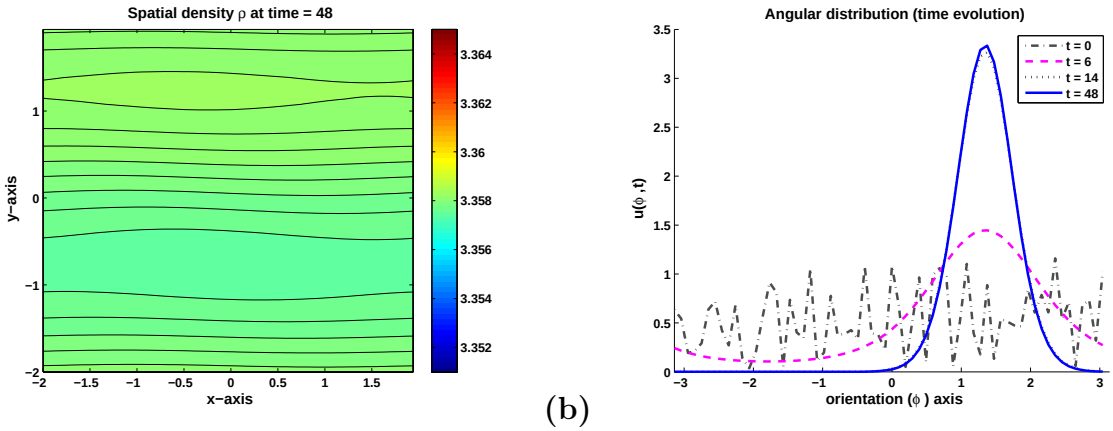

(a) (b)

Figure 5: Run 2 (alignment dominated): $q_r = 1$, $q_{al} = 3$, $q_a = 1$ and $k_r = -0.25$, $k_{al} = 0.75$, $k_a = 0.25$. Attraction and repulsion balance each other, alignment is the principal interaction mechanism. The initial density is the constant 1 plus a uniform random distribution in space and angle. (a) Contour plot of the spatial density ρ at $t = 48$. Note that the density is virtually uniform. (b) Plot of density u as a function of angle ϕ at a fixed location in space at $t = 0$ (dashed-dot), $t = 6$ (dashed), $t = 14$ (dotted) and $t = 48$ (solid). The individuals align along a preferred direction at $\phi = 1.37$ radians (about 78.75 degrees) creating an almost translational group motion. There is no noticeable change in the angular profile beyond $t = 20$.

in the angular profile of the solution after $t = 20$. The alignment of individuals observed in this run is similar to the alignment found in the orientational distribution of actin cells [27], with the caveat that our model considers in addition space-dependence and also attraction and repulsion interaction forces.

The solution depicted in Figure 4 is typical to observations of fish schools moving from one location to another, where behavioral matching is expressed by the tendency of each individual to match its orientation with that of its nearby neighbors (parallel orientation). Swimming in groups can have various advantages, such as enhanced foraging success, increased access to mates, hydrodynamic efficiency and better predator avoidance. We refer to [43] for a brief, but detailed survey of mathematical models for fish schooling, with referrals to the experimental observations that validate the models. Similar alignment behaviors are observed in migrating herds of ungulates [44] or flocks of birds [45].

Remark. By taking the alignment turning function v_{al} (see (24) and (25)) in the form

$$v_{al}(\theta) = k_{al} \sin(2\theta), \tag{52}$$

we obtained numerically a "two-way" translational solution, along two opposite directions, similar to the bipolar angular distributions in actin networks [27]. The function v_{al} from (52) describes alignment at acute interaction ranges and anti-alignment at obtuse angles. A plot similar to Figure 5 (not shown here) would indicate convergence to a spatially homogeneous stationary distribution with *two* peaks of equal height, at π angular distance from each other.

Run 3 (aggregation with alignment): Random in space and direction initial data as in Run 1, with parameters: $q_r = 1$, $q_{al} = 5$, $q_a = 5$ and $k_r = -0.1$, $k_{al} = 0.75$, $k_a = 0.75$. Alignment and attraction dominate in strength the repulsion. Also, the turning, as indicated by the magnitude

of κ_j's, $j = r, al, a$, is primarily driven by alignment and attraction interactions. The individuals aggregate in a group and also align their directions of motion.

Figures 6(a) and 6(c) show the spatial density at $t = 20$ and $t = 35$, respectively. Having started from a random initial distribution, individuals aggregate at $t = 20$. Note the scale on the right-hand-side of Figure 6(a), indicating a density range between 3.55 and 4.6 with a high density group centered at around $(0.09, -1.26)$. At $t = 35$ (Figure 6(c)) we observe the formation of a group with well-defined boundaries, similar to that seen in Run 1 (Figure 4(a)).

Figures 6(b) and 6(d) display, respectively, the angular distribution of the density u at $t = 20$ and $t = 35$, at four space locations. For both figures, the first space location is the point of highest density (solid line). The other three space locations are horizontal translations of the point of highest density, to the right, by $16\Delta x$, $32\Delta x$ and $48\Delta x$ (Figure 6(b)) and $3\Delta x$, $6\Delta x$ and $9\Delta x$ (Figure 6(d)). Note that both figures show an alignment of individuals along the same preferred direction at $\phi = -2.35$ radians (-135 degrees). The individuals have not yet formed a well-defined group by $t = 20$, but they did align along a preferred direction and they maintained that preferred orientation through the aggregation process that took place until $t = 35$. Also note in Figure 6(c) the elongated shape of the group at $t = 35$. The elongation is precisely along the direction of motion, that is $\phi = -135$ degrees.

The solution from Figure 6 combines features from the previous two runs: aggregation into a group with higher density at the core (as in Figure 4) and movement along a preferred direction (as in Figure 5). This pattern may correspond for instance to the prey-flock escaping behavior in response to a predator's attack. According to the selfish herd model [46], the risk of predation is reduced if an individual places himself between another prey individual and the predator. This behavior results in an aggregation that runs away from the predator, with individuals in the center potentially being favored. We refer to [47] and references therein for a recent account on the theoretical, modeling and experimental aspects of the selfish herd concept. Finally, it is interesting to point out that the "tail" behind the moving group (Figure 6) has also been observed in simulations of particle-based models [48].

5 Discussion and future directions

The purpose of this paper is to introduce and make a preliminary investigation on the two-dimensional extension of the nonlocal continuum model for aggregation (1) from [1, 33]. To extend (1) to two dimensions we adopt a kinetic formulation that leads to a generalization of the model of dispersal of organisms derived in [14] using a discrete stochastic approach called velocity jump process. The main novelty in the present model (2) (as adapted from its one-dimensional case (1)) concerns the assumptions we make on the turning rates, to include, nonlocally, the three types of social interactions that act among individuals of a group: attraction, repulsion and alignment. The mathematical model (2) conserves mass, has solutions of bounded amplitude and gradients and reduces nicely (but non-trivially) to the one-dimensional model (1).

The two-dimensional model (2) exhibits several collective behaviors of biological aggregations observed in nature. When attraction is the dominant interaction force and individuals have little or no tendency to align with their neighbors, we observe the formation of a circular swarm group (Figure 4), with a higher density at the center and random drift of the individuals in the swarm. This solution agrees very well to the observations on the structure and dynamics of mosquito swarms [40], in particular the male swarms of *Anopheles gambiae* [41] that form to serve various

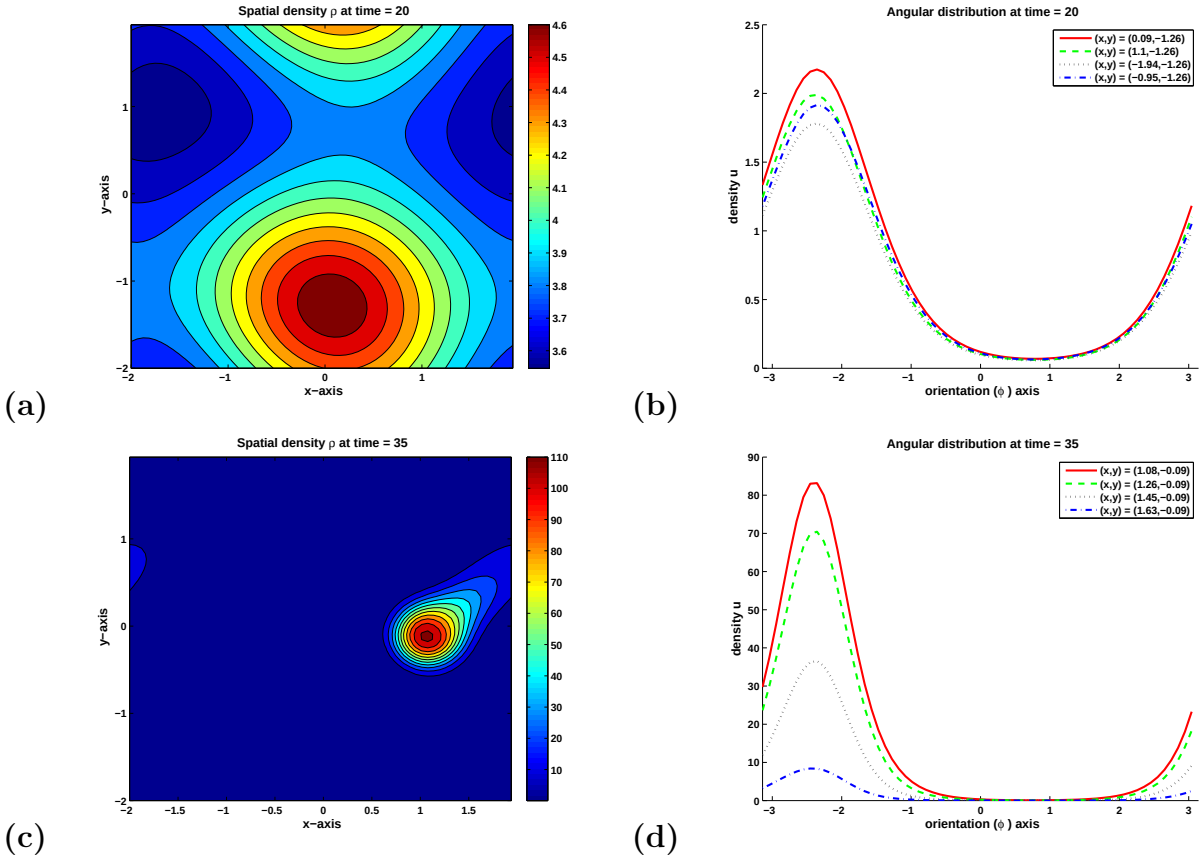

Figure 6: Run 3 (attraction and alignment dominated): $q_r = 1$, $q_{al} = 5$, $q_a = 5$ and $k_r = -0.1$, $k_{al} = 0.75$, $k_a = 0.75$. Random in space and direction initial data. (a) Contour plot of the spatial density ρ at $t = 20$. (b) Angular distribution of the density u at $t = 20$ and four space locations. The solid line corresponds to the highest density point. The other three space locations are horizontal translations of the point of highest density, to the right, by $16\Delta x$, $32\Delta x$ and $48\Delta x$, corresponding to the dashed, dotted and dash-dotted lines, respectively. (c) Contour plot of the spatial density ρ at $t = 35$. (d) Angular distribution of the density u at $t = 35$ and four space locations. The first location is the center of the swarm (solid line). The other three space locations are horizontal translations of the center of the swarm to the right, by $3\Delta x$, $6\Delta x$ and $9\Delta x$, corresponding to the dashed, dotted and dash-dotted lines, respectively. The individuals align along a preferred direction $\phi = -2.35$ radians (-135 degrees) and aggregate in a group with well-defined boundaries. Also note that the shape of the group at $t = 35$ is elongated along the direction of motion.

purposes with respect to mating. Relatively large alignment and low attraction and repulsion interactions result in a spatially homogeneous solution with movement along a preferred direction (Figure 5), similar to patterns observed in migrating schools of fish [43], herds of ungulates [44] or flocks of birds [45]. For attraction and alignment dominated interactions, we observe aggregation into a group that moves along a preferred direction (Figure 6). The pattern may correspond to the escaping behavior of a prey species under the threat of predation, conforming to the selfish herd model [46, 47].

A very interesting aspect of the mathematical modeling is the study of transitions between various group patterns as the model parameters are varied. Studies [1, 33, 34] of (1), the one-dimensional version of our model, showed very interesting transitions between patterns, corresponding to different daily activities of the individuals. For instance [33], by changing the values of several parameters, the model can be used to describe the following succession of activities: forage, rest, travel, then back to forage. Moreover, by changing the parameters back to their previous values one typically observes a hysteresis phenomenon. We expect our model to capture an even more diverse range of state transitions and hysteresis effects and we plan to address such studies in our future work.

The patterns obtained with particle-based models are typically more diverse, as they include milling solutions (turning around in a torus-like formation) [10, 13, 12], rotation clumps, ring and ring clumping patterns [13], etc. Milling formations in particular are mostly observed in schooling fish, such as jack, barracuda and tuna [49, 10]. The occurrence of such mills in nature is a relatively rare event, and this is reflected in the small sets of parameter values for which these solutions are obtained. Figure 3(e) in [10], for instance, maps the parameter space to show the occurrence of four types of patterns obtained with their model: swarm, torus, parallel groups and highly parallel groups. The set of parameters corresponding to the milling solution is much smaller than the rest, making the pattern hard to detect. In future work we want to perform a more extensive numerical exploration of the parameter space for our PDE model (2) to test its capabilities in capturing milling (and other) patterns not presented in the present article.

6 Appendix

$1D$ reduction: calculation of attraction and repulsion components of (42) and (43). Regarding the attraction component of λ, calculate from (10) and (37) that, for a right-moving individual x with $\phi = 0$,

$$\lambda_a(x,0) = q_a \int K_a^d(x-s) K_a^o(s;x,0)(u^+(s,t)+u^-(s,t))\,ds.$$

Recall from (9) that $K_a^o(\mathbf{s};\mathbf{x},\phi)$ depends on the orientation ϕ of $\mathbf{x}$ and the angle ψ that the relative location $\mathbf{s}-\mathbf{x}$ makes with the x-axis. In the one-dimensional setting, for a right-moving individual x with $\phi = 0$, individuals that are ahead have $\psi = 0$, while those behind have $\psi = \pi$. From (9), we have $K_a^o(s;x,0) = 0$ for individuals ahead ($s > x$, $\psi = 0$) and $K_a^o(s;x,0) = 1/\pi$ for individuals behind ($s < x$, $\psi = \pi$). Therefore,

$$\lambda_a(x,0) = q_a \frac{1}{\pi} \int_{-\infty}^{x} K_a^d(x-s)(u^+(s,t)+u^-(s,t))\,ds.$$

Also, from similar arguments,

$$\lambda_a(x,\pi) = q_a \frac{1}{\pi} \int_x^\infty K_a^d(x-s)(u^+(s,t)+u^-(s,t))\,ds.$$

The attraction components of $T(x,0,\phi)$ and $T(x,\pi,\phi)$ can be computed from (18), using (37):

$$T_a(x,0,\phi) = q_a \frac{1}{\pi} \int_{-\infty}^x K_a^d(x-s)\left(w_a(0-\phi,0-0)u^+(s,t) + w_a(0-\phi,0-\pi)u^-(s,t)\right)\,ds,$$

and

$$T_a(x,\pi,\phi) = q_a \frac{1}{\pi} \int_x^\infty K_{al}^d(x-s)\left(w_a(\pi-\phi,\pi-0)u^+(s,t) + w_a(\pi-\phi,\pi-\pi)u^-(s,t)\right)\,ds.$$

Here we used again that $K_a^o(s;x,0)$ yields 0 if s is ahead of x ($s > x$, $\psi = 0$) and $\frac{1}{\pi}$ provided s is behind x ($s < x$, $\psi = \pi$), with similar considerations for $K_a^o(s;x,\pi)$.

Assume that an individual turns to meet another individual whenever an attractive-type interaction occurs. This implies that the turning probability functions w_a is in the form

$$w_a(\phi'-\phi,\phi'-\psi) = \delta(\phi-\phi'-\pi).$$

The equation describes the fact that an individual x moving in the direction ϕ' interacts with the individual s behind him and turns to direction ϕ to meet him. From these considerations we conclude:

$$T_a(x,0,\phi) = \delta(\phi-\pi) q_a \frac{1}{\pi} \int_{-\infty}^x K_a^d(x-s)\left(u^+(s,t)+u^-(s,t)\right)\,ds,$$
$$T_a(x,\pi,\phi) = \delta(\phi) q_a \frac{1}{\pi} \int_x^\infty K_{al}^d(x-s)\left(u^+(s,t)+u^-(s,t)\right)\,ds.$$

We further infer that

$$T_a(x,0,\phi) = \delta(\phi-\pi)\lambda_a(x,0)$$
$$T_a(x,\pi,\phi) = \delta(\phi)\lambda_a(x,\pi).$$

Upon substitution in (43) with use of (39) we conclude that the attraction component of the expression given by (43) equals that of (42).

The repulsion components can be treated in an analogous fashion. We omit the details.

Acknowledgment

The author was supported by NSERC RGPIN-341834. The author thanks Raluca Eftimie for suggesting this problem to him and for the stimulating discussions during this research.

References

[1] R. Eftimie, G. de Vries, M. A. Lewis, F. Lutscher, Modeling group formation and activity patterns in self-organizing collectives of individuals, Bull. Math. Biol. 69 (5) (2007) 1537–1566.

[2] S. Camazine, J.-L. Deneubourg, N. R. Franks, J. Sneyd, G. Theraulaz, E. Bonabeau, Self-organization in biological systems, Princeton Studies in Complexity, Princeton University Press, Princeton, NJ, 2003, reprint of the 2001 original.

[3] T. Feder, Statistical physics is for the birds, Physics Today 60 (10) (2007) 28–30.

[4] J. K. Parrish, L. E. Keshet, Complexity, pattern, and evolutionary trade-offs in animal aggregation, Science 284 (1999) 99–101.

[5] R. Lukeman, Y.-X. Li, L. Edelstein-Keshet, A conceptual model for milling formations in biological aggregates, Bull. Math. Biol. 71 (2) (2009) 352–382.

[6] J. K. Parrish, Using behavior and ecology to exploit schooling fishes, Environ. Biol. Fish. 55 (1999) 157–181.

[7] A. B. T. Barbaro, K. Taylor, P. F. Trethewey, L. Youseff, B. Birnir, Discrete and continuous models of the dynamics of pelagic fish: application to the capelin, Math. Comput. Simulation 79 (12) (2009) 3397–3414.

[8] S. J. Simpson, A. R. McCaffery, B. F. Hägele, A behavioural analysis of phase change in the desert locust, Biol. Rev. 74 (1999) 461–480.

[9] T. Vicsek, A. Czirók, E. Ben-Jacob, I. Cohen, O. Shochet, Novel type of phase transition in a system of self-driven particles, Phys. Rev. Lett. 75 (6) (1995) 1226–1229.

[10] I. D. Couzin, J. Krause, R. James, G. Ruxton, N. R. Franks, Collective memory and spatial sorting in animal groups, J. Theor. Biol. 218 (2002) 1–11.

[11] F. Cucker, S. Smale, Emergent behavior in flocks, IEEE Trans. Automat. Control 52 (5) (2007) 852–862.

[12] H. Levine, W.-J. Rappel, I. Cohen, Self-organization in systems of self-propelled particles, Phys. Rev. E 63 (1) (2000) 017101.

[13] M. R. D'Orsogna, Y.-L. Chuang, A. L. Bertozzi, L. S. Chayes, Self-propelled particles with soft-core interactions: patterns, stability and collapse, Phys. Rev. Lett. 96 (10) (2006) 104302.

[14] H. G. Othmer, S. R. Dunbar, W. Alt, Models of dispersal in biological systems, J. Math. Biol 26 (1988) 263–298.

[15] A. Mogilner, L. Edelstein-Keshet, A non-local model for a swarm, J. Math. Biol. 38 (1999) 534–570.

[16] C. M. Topaz, A. L. Bertozzi, M. A. Lewis, A nonlocal continuum model for biological aggregation, Bull. Math. Bio. 68 (2006) 1601–1623.

[17] F. Lutscher, Modeling alignment and movement of animals and cells, J. Math. Biol. 45 (2002) 234–260.

[18] B. Pfistner, A one dimensional model for the swarming behavior of Myxobakteria, in: W. Alt, G. Hoffmann (Eds.), Biological Motion, Lecture Notes on Biomathematics, 89, Springer, 1990, pp. 556–563.

[19] N. Bellomo, H. Berestycki, F. Brezzi, J.-P. Nadal, Mathematics and complexity in life and human sciences, Math. Models Methods Appl. Sci. DOI: 10.1142/S0218202510004702.

[20] P. Degond, S. Motsch, Continuum limit of self-driven particles with orientation interaction, Math. Models Methods Appl. Sci. 18 (suppl.) (2008) 1193–1215.

[21] S.-Y. Ha, E. Tadmor, From particle to kinetic and hydrodynamic descriptions of flocking, Kinet. Relat. Models 1 (3) (2008) 415–435.

[22] C. Cercignani, R. Illner, M. Pulvirenti, The mathematical theory of dilute gases, Vol. 106 of Applied Mathematical Sciences, Springer-Verlag, New York, 1994.

[23] Y.-L. Chuang, M. R. D'Orsogna, D. Marthaler, A. L. Bertozzi, L. S. Chayes, State transitions and the continuum limit for a 2D interacting, self-propelled particle system, Phys. D 232 (1) (2007) 33–47.

[24] A. L. Bertozzi, J. A. Carrillo, T. Laurent, Blow-up in multidimensional aggregation equations with mildly singular interaction kernels, Nonlinearity 22 (3) (2009) 683–710.

[25] K. Fellner, G. Raoul, Stable stationary states of non-local interaction equations, Mathematical Models and Methods in Applied Sciences (M3AS) (to appear).

[26] T. Hillen, A. Stevens, Hyperbolic models for chemotaxis in 1-D, Nonlinear Analysis: Real World Applications 1 (2000) 409–433.

[27] E. Geigant, K. Ladizhansky, A. Mogilner, An integrodifferential model for orientational distributions of F-actin in cells, SIAM J. Appl. Math. 59 (3) (1998) 787–809.

[28] L. Edelstein-Keshet, B. Ermentrout, Models for contact-mediated pattern formation: cells that form parallel arrays, J. Math. Biol. 29 (1990) 33–58.

[29] B. Pfistner, W. Alt, A two dimensional random walk model for swarming behavior, in: W. Alt, G. Hoffmann (Eds.), Biological Motion, Lecture Notes on Biomathematics, 89, Springer, 1990, pp. 564–565.

[30] A. Mogilner, L. Edelstein-Keshet, Selecting a common direction. I. How orientational order can arise from simple contact responses between interacting cells, J. Math. Biol. 33 (1995) 619–660.

[31] A. Mogilner, L. Edelstein-Keshet, G. B. Ermentrout, Selecting a common direction. II. Peak-like solutions representing total alignment of cell clusters, J. Math. Biol. 34 (1996) 811–842.

[32] A. Mogilner, L. Edelstein-Keshet, Spatio-angular order in populations of self-aligning objects: formation of oriented patches, Physica D 89 (1996) 346–367.

[33] R. Eftimie, G. de Vries, M. A. Lewis, Complex spatial group patterns result from different animal communication mechanisms, Proc. Natl. Acad. Sci. 104 (17) (2007) 6974–6979.

[34] R. Eftimie, G. de Vries, M. Lewis, Weakly nonlinear analysis of a hyperbolic model for animal group formation, J. Math. Biol. 59 (2009) 37–74.

[35] R. C. Fetecau, R. Eftimie, An investigation of a nonlocal hyperbolic model for self-organization of biological groups, J. Math. Biol. 61 (4) (2009) 545–579.

[36] J. A. Carrillo, M. Fornasier, J. Rosado, G. Toscani, Asymptotic flocking dynamics for the kinetic Cucker-Smale model, SIAM J. Math. Anal. 42 (1) (2010) 218–236.

[37] M. Ballerini, N. Cabibbo, R. Candelier, A. Cavagna, E. Cisbani, I. Giardina, V. Lecomte, A. Orlandi, G. Parisi, A. Procaccini, M. Viale, V. Zdravkovic, Interaction ruling animal collective behaviour depends on topological rather than metric distance: evidence from a field study, Proc. Natl. Acad. Sci. 105 (2008) 1232–1237.

[38] A. Cavagna, A. Cimarelli, I. Giardina, G. Parisi, R. Santagati, F. Stefanini, R. Tavarone, From empirical data to inter-individual interactions: unveiling the rules of collective animal behavior, Math. Models Methods Appl. Sci. DOI: 10.1142/S0218202510004660.

[39] C. Canuto, M. Y. Hussaini, A. Quarteroni, T. A. Zang, Spectral methods in fluid dynamics, Springer Series in Computational Physics, Springer-Verlag, New York, 1988.

[40] A. Okubo, D. Grünbaum, L. Edelstein-Keshet, The dynamics of animal grouping, in: Okubo A., Levin S., Diffusion and ecological problems: modern perspectives, Springer, N.Y., 2001, pp. 197–237.

[41] N. C. Manoukis, A. Diabate, A. Abdoulaye, M. Diallo, A. Dao, A. Yaro, J. M. Ribeiro, T. Lehmann, Structure and dynamics of male swarms of *anopheles gambiae*, J. Med. Entomol. 46 (2) (2009) 227–235.

[42] H. R. Bullis, Observations on the feeding behavior of white-tip sharks on schooling fishes, Ecology 42 (1961) 194–195.

[43] J. K. Parrish, S. V. Viscido, D. Grunbaum, Self-organized fish schools: An examination of emergent properties, Bioll. Bull. 202 (2002) 296–305.

[44] A. Sinclair, M. Norton-Griffiths, Serengeti: Dynamics of an ecosystem, University of Chicago Press, 1979.

[45] F. H. Heppner, Animal Groups in Three Dimensions, Cambridge University Press, 1997, Ch. Three-dimensional structure and dynamics of birds flocks.

[46] W. D. Hamilton, Geometry for the selfish herd, J. Theor. Biol. 31 (1971) 295–311.

[47] S. V. Viscido, The case for the selfish herd hypothesis, Comments on theoretical biology 8 (2003) 665–684.

[48] J. Gautrais, C. Jost, G. Theraulaz, Key behavioural factors in a self-organised fish school model, Ann. Zool. Fennici 45 (2008) 415428.

[49] J. K. Parish, S. V. Viscido, D. Grunbaum, Self-organized fish schools: an examination of emergent properties, Biol. Bull. 202 (2002) 296–305.